Activation of the AMPK-FOXO3 Pathway Reduces Fatty Acid–Induced Increase in Intracellular Reactive Oxygen Species by Upregulating Thioredoxin

Xiao-Nan Li,[1,2,3] Jun Song,[1,2,3] Lin Zhang,[1,2] Scott A. LeMaire,[1,2] Xiaoyang Hou,[1,2,3] Cheng Zhang,[1,2,3] Joseph S. Coselli,[1,2] Li Chen,[3] Xing Li Wang,[1,2] Yun Zhang,[3] and Ying H. Shen[1,2]

OBJECTIVE—Oxidative stress induced by free fatty acids contributes to the development of cardiovascular diseases in patients with metabolic syndrome. Reducing oxidative stress may attenuate these pathogenic processes. Activation of AMP-activated protein kinase (AMPK) has been reported to reduce intracellular reactive oxygen species (ROS) levels. The thioredoxin (Trx) system is a major antioxidant system. In this study, we investigated the mechanisms involved in the AMPK-mediated regulation of Trx expression and the reduction of intracellular ROS levels.

RESEARCH DESIGN AND METHODS—We observed that activation of AMPK by 5-aminoimidazole-4-carboxamide ribonucleotide (AICAR) significantly reduced ROS levels induced by palmitic acid in human aortic endothelial cells. Activation of AMPK increased expression of the antioxidant Trx, which mediated the ROS reduction. RT-PCR showed that AMPK regulated Trx at the transcriptional level.

RESULTS—Forkhead transcription factor 3 (FOXO3) was identified as the target transcription factor involved in the upregulation of Trx expression. FOXO3 bound to the *Trx* promoter, recruited the histone acetylase p300 to the *Trx* promoter, and formed a transcription activator complex, which was enhanced by AICAR treatment. AMPK activated FOXO3 by promoting its nuclear translocation. We further showed that AICAR injection increased the expression of Trx and decreased ROS production in the aortic wall of ApoE−/− mice fed a high-fat diet.

CONCLUSIONS—These results suggest that activation of the AMPK-FOXO3 pathway reduces ROS levels by inducing Trx expression. Thus, the AMPK-FOXO3-Trx axis may be an important defense mechanism against excessive ROS production induced by metabolic stress and could be a therapeutic target in treating cardiovascular diseases in metabolic syndrome. ***Diabetes*** **58:2246–2257, 2009**

From the [1]Division of Cardiothoracic Surgery, Michael E. DeBakey Department of Surgery, Baylor College of Medicine, Houston, Texas; the [2]Texas Heart Institute at St. Luke's Episcopal Hospital, Houston, Texas; and [3]Qilu Hospital, Shandong University, Jinan, Shandong, China.

Corresponding authors: Yun Zhang, zhangyun@sdu.edu.cn, and Ying H. Shen, hyshen@bcm.edu.

Received 31 October 2008 and accepted 28 June 2009.

Published ahead of print at http://diabetes.diabetesjournals.org on 10 July 2009. DOI: 10.2337/db08-1512.

X.-N.L. and J.S. contributed equally to this study.

Oxidative stress induced by free fatty acids (FFAs) plays a key role in the development of cardiovascular diseases in metabolic syndrome (1). Excessive generation of reactive oxygen species (ROS) can cause cellular injury and dysfunction by directly oxidizing and damaging DNA, proteins, and lipids, as well as by activating several cellular stress-signaling and inflammatory pathways (1). Understanding how ROS production and scavenging are regulated and developing strategies to reduce ROS production and increase antioxidant availability are important for preventing cardiovascular diseases in metabolic syndrome.

An important signaling pathway involved in ROS regulation is the AMP-activated protein kinase (AMPK) pathway. The AMPK pathway responds to energy depletion by stimulating ATP production, and it plays an important role in controlling energy metabolism. It has been increasingly recognized that activation of this pathway could protect the cardiovascular system (2–4). ROS can activate the AMPK pathway (5–7). Previous studies have shown that activation of the AMPK pathway reduces intracellular ROS levels (7–10). However, the mechanisms involved are not completely understood.

The thioredoxin (Trx) system is a major antioxidant system, which promotes the reduction of proteins by cysteine thiol-disulfide exchange, and plays a vital role in maintaining the cellular redox balance (11,12). Trx, a 12 kDa redox-sensitive molecule, is the key component of the system (11,12). Trx is ubiquitously expressed and protects the cells from ROS-induced cytotoxicity (13–15). Trx has been shown to have cardiovascular protective effects. Inhibition of endogenous Trx in the heart increases oxidative stress and cardiac hypertrophy (16), whereas overexpression of Trx (15,17) or administration of exogenous Trx (18) reduces oxidative stress and protects the cardiovascular system.

Given the importance of Trx in the intracellular antioxidant defense system, we postulate that Trx is a key AMPK target that attenuates excess ROS produced by metabolic stress. Therefore, in the present study, we examined the effect of activating the AMPK pathway on Trx expression and ROS reduction in cells exposed to palmitic acid.

RESEARCH DESIGN AND METHODS

Cell culture. Human aortic endothelial cells (HAECs) (Cell Applications, San Diego, CA) were cultured in EGM-2 media (Cambrex, East Rutherford, NJ), which contained endothelial cell basic media, 2% FBS, hydrocortisone, fibroblast growth factor 2, vascular endothelial growth factor, IGF-I, epidermal growth factor, ascorbic acid, GA-1000, and heparin. The cells were transfected with small interfering RNAs (siRNAs) or plamid DNAs or treated

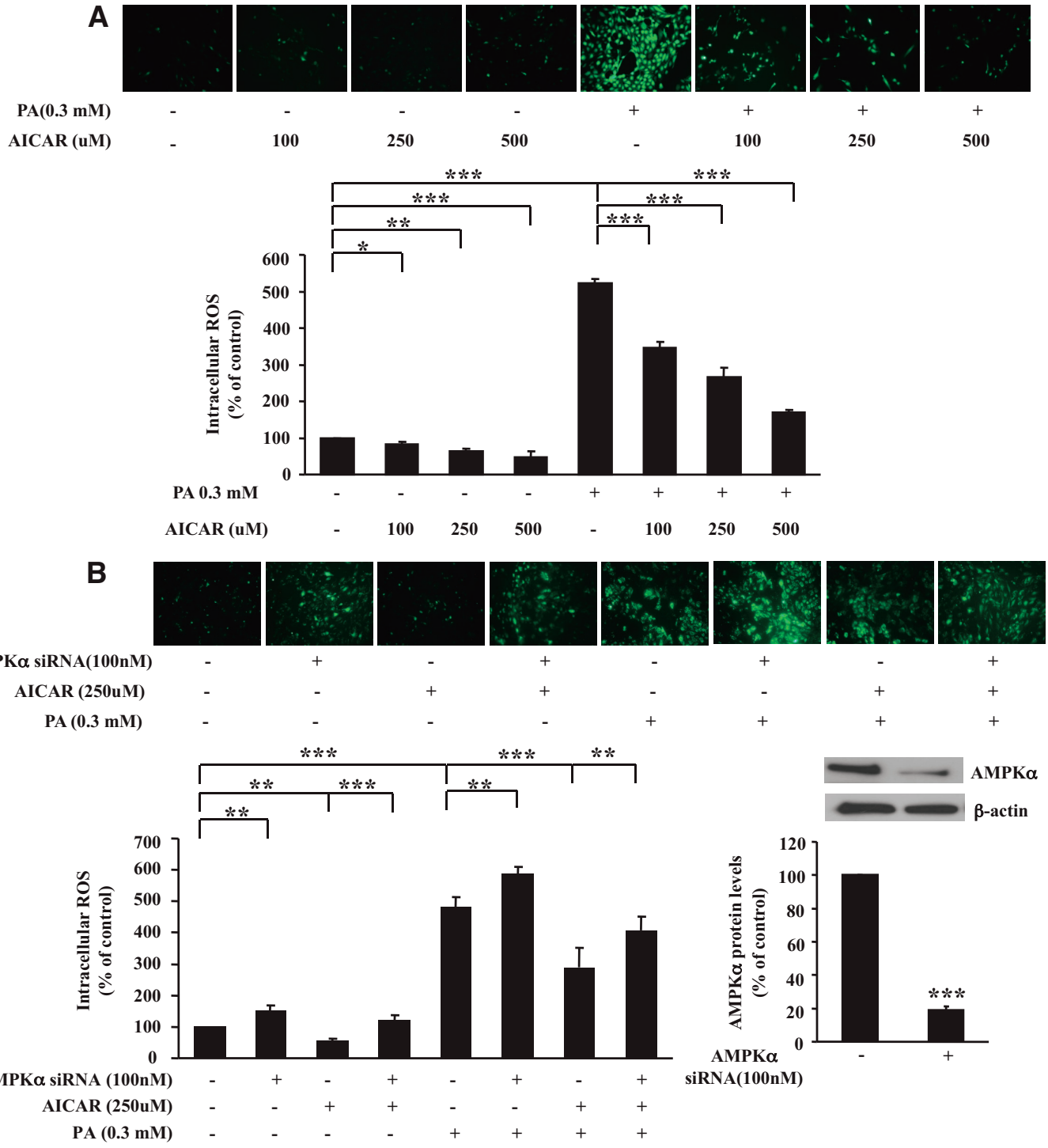

FIG. 1. Activation of the AMPK pathway reduced intracellular ROS levels induced by palmitic acid (PA). *A*: AICAR significantly reduced palmitic acid-increased intracellular ROS levels in HAECs. The cells were treated with AICAR in the absence or presence of palmitic acid for 24 h and then incubated with CM-H_2DCFDA. Fluorescence was detected and normalized to cell number. The mean fluorescent intensity was calculated randomly from five fields per coverslip. Relative ROS levels were compared with the nontreatment control subjects and expressed as the percentage of the control subjects. Shown are representative microscopic scans and the quantitative analysis of fluorescent intensity from three independent experiments. Data represent means ± SE. *$P < 0.05$, **$P < 0.01$, ***$P < 0.001$. *B*: AMPK was involved in the AICAR-induced reduction in ROS levels. HAECs were transfected with AMPK siRNA and then treated with AICAR in the absence or presence of palmitic acid for 24 h. The effectiveness of AMPKα knockdown was examined by anti-AMPKα antibody. ROS were detected with CM-H_2DCFDA. Representative staining and the quantitative analysis are shown. Data represent the means ± SE ($n = 3$). **$P < 0.01$ ***$P < 0.001$. AMPKα siRNA prevented AICAR-induced reduction of ROS. (A high-quality digital representation of this figure is available in the online issue.)

with AICAR or palmitic acid at various concentrations and for the time indicated.

Preparation of fatty acid–albumin complexes. Saturated palmitic acid was used in this study. We prepared lipid-containing media by conjugating palmitic acid to BSA using a modification of the method described previously (19). Briefly, palmitic acid was dissolved in ethanol at 200 mmol/l and then combined with 10% FFA-free, low-endotoxin BSA, giving a final concentration of 1 to 5 mmol/l. The pH of all solutions was adjusted to ~7.5, and the stock solutions were filter-sterilized and stored at −20°C until used. Control solutions containing ethanol and BSA were prepared similarly.

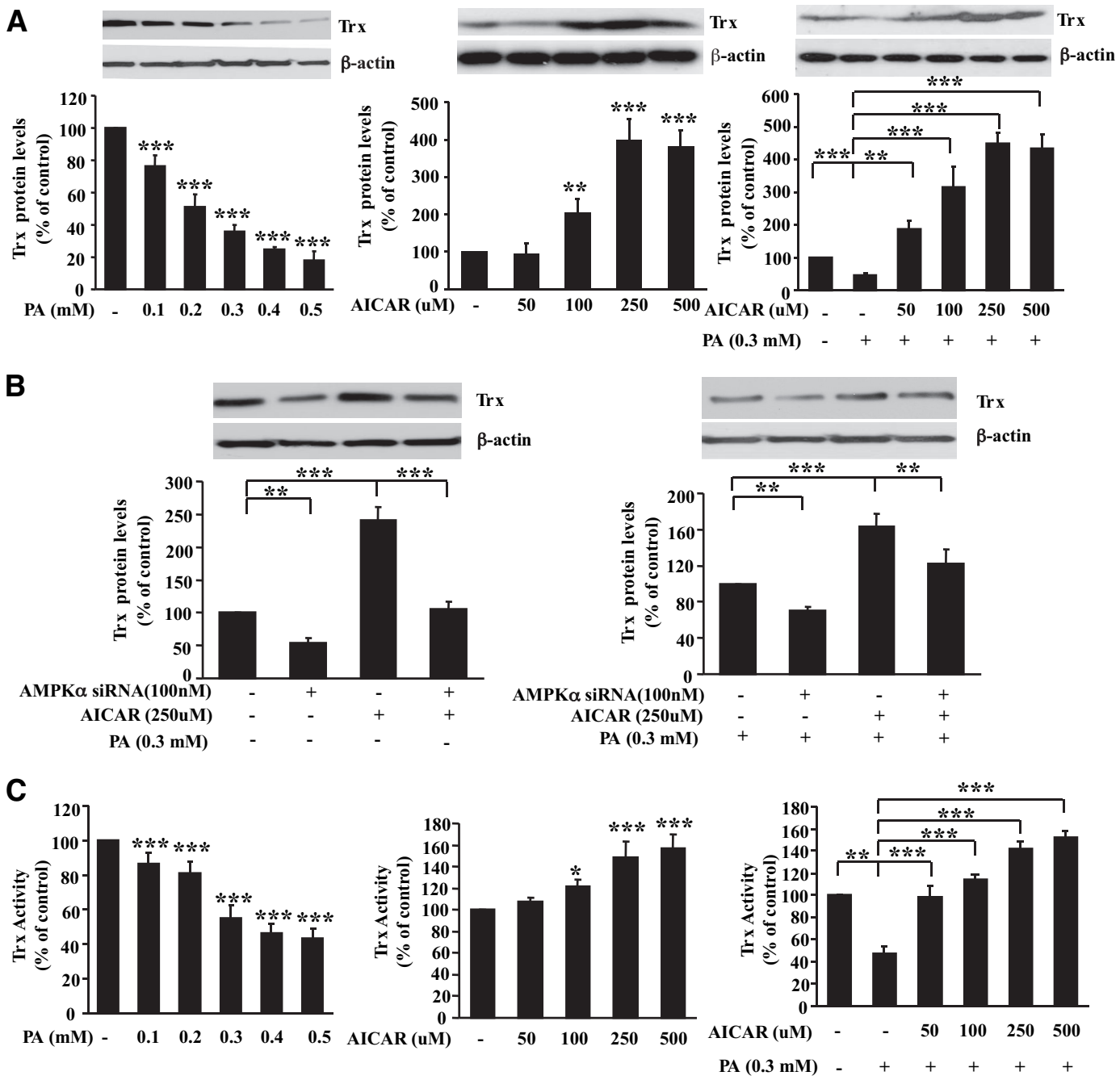

FIG. 2. Activation of the AMPK pathway upregulated Trx. *A*: AICAR induced Trx expression in the absence or the presence of palmitic acid (PA). HAECs were treated with increasing amounts of palmitic acid, AICAR, or palmitic acid and AICAR for 24 h. Trx expression was examined by an anti-Trx antibody on a Western blot and was normalized with β-actin. The relative levels of Trx were compared and expressed as the percentage of the control. Representative blots and quantitative analysis from three independent experiments are shown. **$P < 0.01$, ***$P < 0.001$ versus nontreatment control subjects or as indicated. *B*: Involvement of the AMPK pathway in basal and AICAR-regulated Trx expression. HAECs were transfected with AMPK siRNAs and then treated with AICAR in the absence or presence of palmitic acid for 24 h. Trx expression was measured by an anti-Trx antibody on a Western blot and was normalized with β-actin. The relative levels of protein were compared and expressed as the percentage of the control. Representative blots and quantitative analysis from three independent experiments are shown. **$P < 0.01$, ***$P < 0.001$ versus the nontreatment control subjects or as indicated. Knockdown of AMPKα by siRNA downregulated basal Trx protein levels and reversed the AICAR-induced induction of Trx. *C*: AICAR enhanced total Trx activity. HAECs were treated with increasing amounts of palmitic acid, AICAR, or palmitic acid and AICAR for 24 h. Relative Trx activity in the cell lysate was assessed, normalized, and expressed as the percentage of the nontreatment control subjects. Data represent the means ± SE ($N = 3$). *$P < 0.05$, **$P < 0.01$, ***$P < 0.001$ versus the nontreatment control subjects or as indicated.

Working solutions were prepared fresh by diluting the stock solution (1:10) in 2% FCS–endothelial cell basic media. All palmitic acid media contained 1% BSA; however, the palmitic acid–to–BSA ratio varied with the palmitic acid concentration.

siRNA and plasmid DNA transfection. Gene expression was silenced with specific siRNAs, including AMPK siRNA (Santa Cruz Biotechnology, Santa Cruz, CA), Trx siRNA (Santa Cruz Biotechnology), and forkhead transcription factor 3 (FOXO3) siRNA (Dharmacon, Chicago, IL). Various FOXO3a plasmids (Addgene, Cambridge, MA), including wild type (HA-FOXO3a WT), constitutively active (HA-FOXO3a TM), and dominant-negative (HA-FOXO3a TM deltaDB) DNAs were used in this study. Transfection of HAECs or human smooth muscle cells (HSMCs) with siRNAs or plasmid DNAs was carried out with Lipofectamine 2000 (Invitrogen, Carlsbad, CA) according to the manufacturer's instructions. Transfected cells were then treated with palmitic acid

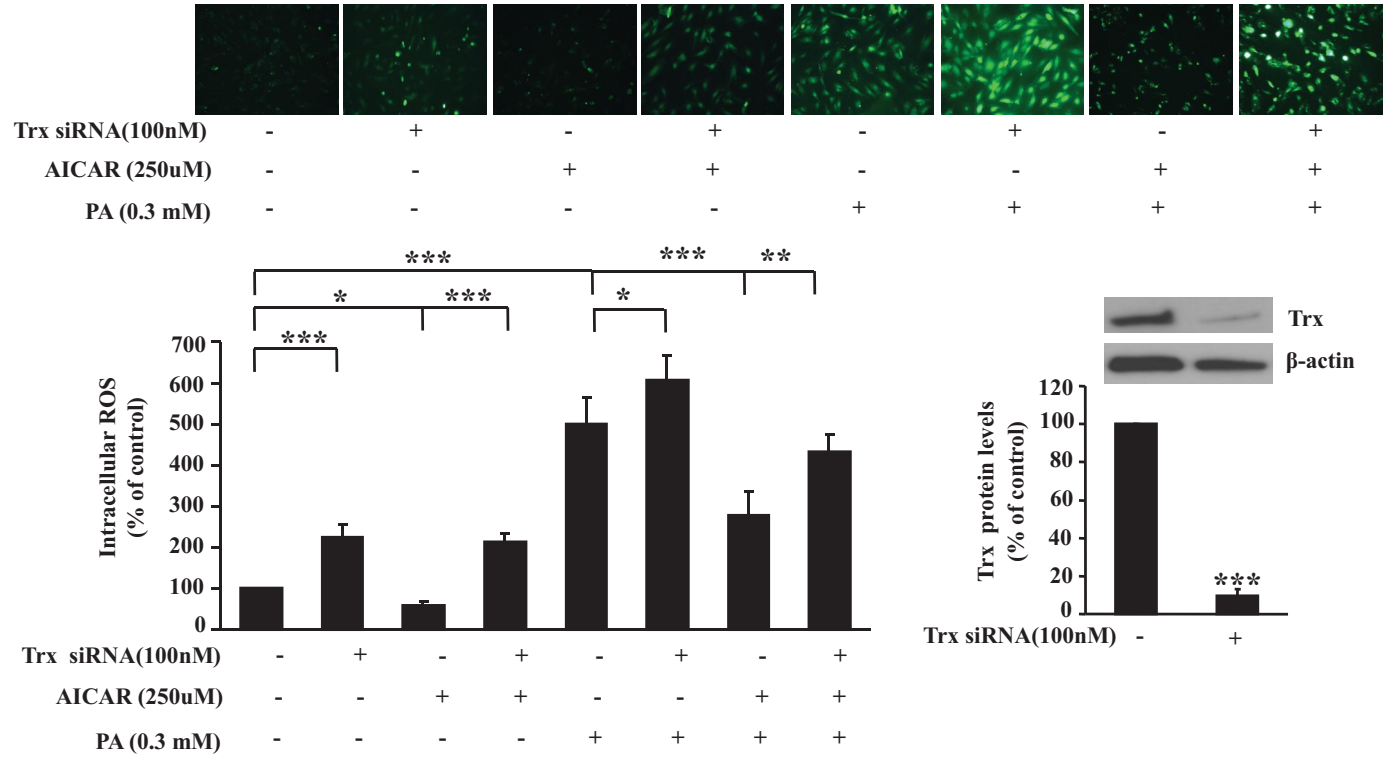

FIG. 3. Trx mediated the AMPK-induced reduction in ROS levels. HAECs were transfected with Trx siRNA and then treated with AICAR in the absence or the presence of palmitic acid (PA) for 24 h. The effectiveness of Trx knockdown was examined by anti-Trx antibody. Intracellular ROS levels were detected with CM-H_2DCFDA. Shown are representative microscopic scans and the quantitative analysis of fluorescent intensity from three experiments. Data represent the means ± SE. *$P < 0.05$, **$P < 0.01$, ***$P < 0.001$. Knockdown of Trx by siRNA increased basal ROS levels, enhanced palmitic acid–induced ROS levels, and prevented the AICAR-induced reduction in ROS levels. (A high-quality digital representation of this figure is available in the online issue.)

and AICAR at the designated concentrations for the indicated amount of time. The efficiency of transfection was confirmed by Western blot.

Quantitative ROS detection. Intracellular ROS levels were detected with the oxidant-sensitive fluorogenic probes 5- (and -6) -chloromethyl-2′,7′-dichlorodihydrofluorescein diacetate, acetyl ester (CM-H_2DCFDA). Treated cells on the coverslip were incubated with 5 μmol/l CM-H_2DCFDA in serum-free medium for 30 min at 37°C. The slides were examined under a Leica DMLS epifluorescence microscope (Leica Microsystems, Bannockburn, IL), the images were captured with a Leica DC 100 digital camera using identical acquisition settings, and the data were analyzed with Image-Pro Plus V4.5 software (Media Cybernetics, Bethesda, MD). Fluorescence was detected and normalized to cell number. The mean fluorescent intensity was calculated randomly from five visual fields per coverslip. Relative ROS levels were compared and expressed as the percentage of the nontreatment control subjects.

Tissue ROS levels were detected with DHE. Fresh segments of thoracic aorta were frozen in optimal cutting temperature compound. Cryosections (6 μm) were equilibrated with Krebs-HEPES buffer (130 mmol/l NaCl, 5.6 mmol/l KCl, 2 mmol/l $CaCl_2$, 0.24 mmol/l $MgCl_2$, 11 mmol/l glucose, and 8.3 mmol/l HEPES; pH 7.4) at 37°C for 30 min. Cryosections were incubated with 2 μmol/l DHE at 37°C for 30 min and stained with the nuclear counterstain DAPI (0.1 μg/ml) at room temperature for 5 min. Fluorescence was detected and all images were captured with identical acquisition parameters. Values of red ethidium fluorescence were normalized to blue DAPI fluorescence. The mean fluorescent intensity randomly counted from three visual fields per vessel was calculated.

Immunofluorescent staining and immunohistochemistry. Cells were grown on glass coverslips and treated with palmitic acid and AICAR. Treated cells were washed with PBS, fixed with 4% paraformaldehyde for 10 min, and permeabilized with 0.2% Triton X-100 for 5 min. The coverslips were blocked with 1% BSA, incubated with the primary antibody, washed with PBS, incubated with Texas Red–labeled secondary antibody, and then stained with 0.1 μg/ml DAPI at room temperature for 5 min. Fluorescence was detected.

For immunohistochemical analysis, formalin-fixed, paraffin-embedded aortic sections were deparaffinized and rehydrated before antigen retrieval in citrate buffer (92–98°C for 12 min). Endogenous peroxidase activity was quenched by incubating the slides with 3% hydrogen peroxide for 10 min, and nonspecific staining was reduced by blocking with 5% normal blocking horse serum. The sections were incubated with the primary antibodies at 4°C overnight and then incubated with second antibody and detected with 3,3-diaminoben zidine (DAB) using the VECTASTAIN ABC kit (Vector Laboratories, Burlingame, CA). Nuclei were counterstained with hematoxylin. Slides treated only with normal IgG were used as negative controls. The images were captured and analyzed with Image-Pro Plus V4.5 software (Media Cybernetics). The signal density was normalized to vascular area. The mean intensity was calculated randomly from three visual fields per vessel.

Western blot analysis. Treated cells were collected and lysed as described previously (20). The NE-PER nuclear and cytoplasmic extraction kit (Thermo Fisher Scientific, Rockford, IL) was used to separate and prepare nuclear and cytoplasmic proteins from cultured HAECs. Protein samples (15 μg per lane) were subjected to SDS-PAGE and transferred to polyvinylidene fluoride (PVDF) membranes. The membranes were blocked, incubated with primary antibody, washed, and incubated with the secondary HRP-labeled antibody. Bands were visualized with enhanced chemiluminescence (Amersham Biosciences, Piscataway, NJ). Protein bands, including β-actin, were quantified by densitometry with the Quantity One imaging program (Bio-Rad, Hercules, CA). The relative protein levels were normalized to β-actin and expressed as the percentage of the nontreatment control subjects.

Quantitative RT-PCR. Total RNA from treated cells was extracted with Trizol (Invitrogen) according to the manufacturer's protocol. The mRNAs were reverse-transcribed with the iScript cDNA synthesis kit (Bio-Rad). Quantitative RT-PCR (qRT-PCR) was performed with the iCycler iQ RT-PCR detection system (Bio-Rad). Primers were designed with Beacon Designer 2.0 software (Premier Biosoft International, Palo Alto, CA). We used the following primers for human Trx: forward 5′-GCCTTGCAAAATGATCAAGC-3 and reverse 5′-TTGGCTCCAGAAAATTCACC-3′. mRNA levels were acquired by normalizing the threshold cycle (Ct) of *Trx* to the Ct of *β-actin*. The relative levels of mRNA were compared and expressed as the percentage of the nontreatment control subjects.

Chromatin immunoprecipitation assay. We used the chromatin immunoprecipitation (ChIP) assay kit (Upstate Biotechnology, Lake Placid, NY) as described previously (20). The immunoprecipitated DNA and the input DNA were quantified with the qRT-PCR detection system (Bio-Rad). The relative

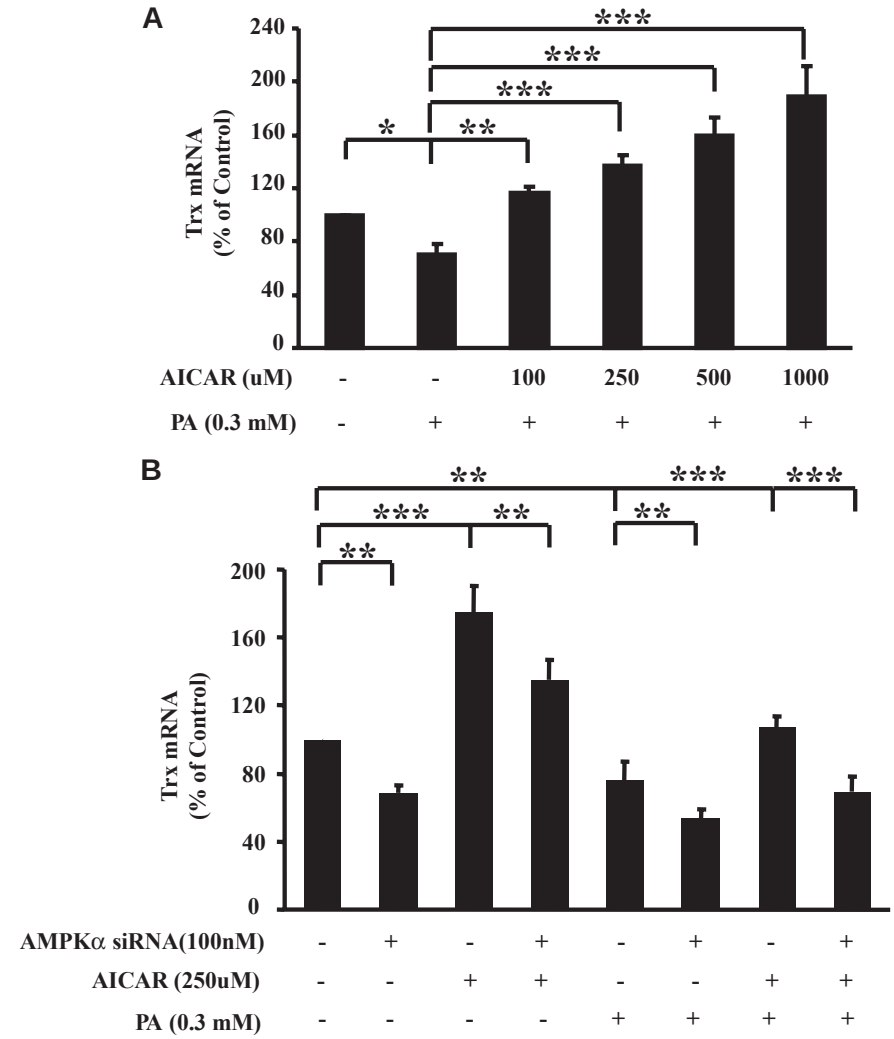

FIG. 4. AMPK induced Trx expression at the transcriptional level. *A*: AICAR induced a significant dose-dependent increase in Trx mRNA. HAECs were treated with AICAR in the presence of palmitic acid (PA) for 24 h. Trx mRNA levels were examined by RT-PCR and normalized with β-actin mRNA. The relative levels of mRNA were compared and expressed as the percentage of the control. Data represent the means ± SE ($N = 3$). *$P < 0.05$, **$P < 0.01$, ***$P < 0.001$ versus palmitic acid treatment. *B*: Involvement of the AMPK pathway in basal and AICAR-regulated Trx expression. HAECs were transfected with AMPK siRNAs and then treated with AICAR in the absence or the presence of palmitic acid for 24 h. Trx mRNA levels were examined by RT-PCR. Data represent the means ± SE ($N = 3$). **$P < 0.01$, ***$P < 0.001$. The basal and AICAR-upregulated Trx mRNA were reversed by AMPK siRNA.

levels of DNA were normalized to the input DNA and expressed as the percentage of the nontreatment control. The PCR products were also separated on a 1.5% agarose gel. The following primers were used for the FOXO binding site in the 5′-flanking region of the human *Trx* gene: for site 6 forward primer 5′-CCGCACTAAACCGCTGTGTC-3′ and reverse primer 5′-CTCCGGAATTTACCGTGACC-3′.

Immunoprecipitation. Immunoprecipitation was conducted as described previously (21). Treated cells were lysed for 60 min in ice-cold extraction buffer containing 50 mmol/l Tris-Cl (pH 7.5), 100 mmol/l NaCl, 1% Triton X-100, 1 mmol/l dithiothreitol, 1 mmol/l EDTA, 1 mmol/l EGTA, 2 mmol/l Na_3VO_4, 50 mmol/l β-glycerophosphate, and a protease inhibitor mixture (Amersham Biosciences). Cleared cell lysates were incubated with the appropriate antibody precoupled to protein A/G-agarose beads (Santa Cruz Biotechnology) at 4°C overnight. The beads were washed twice with extraction buffer and then twice with extraction buffer containing 0.5 mol/l LiCl. Proteins were eluted either in kinase buffer for the kinase assay or in SDS sample buffer for Western blot analysis.

Kinase assays. AMPK was precipitated from cell lysates with an anti-AMPK antibody. AMPK-containing beads were incubated with recombinant FOXO3 in kinase assay buffer supplemented with 100 μmol/l ATP for 20 min at 30°C. Samples were separated on a 10% SDS-PAGE and transferred to PVDF membranes. Anti-serine and anti-threonine antibodies were used to detect phosphorylated serines and threonines incorporated into FOXO3.

Trx activity assay. Trx activity was measured with the insulin disulfide reduction assay as described elsewhere (22). Total cellular protein was extracted with lysis buffer (20 mmol/l HEPES pH 7.9, 100 mmol/l KCl, 300 mmol/l NaCl, 10 mmol/l EDTA, 0.1% Triton X-100, 1 mg/ml Protease Inhibitor Cocktail III). Cellular protein extracts were incubated with buffer (50 mmol/l HEPES pH 7.6, 1 mmol/l EDTA, 1 mg/ml BSA, 2 mmol/l DTT) at 37°C for 15 min before they were incubated with Trx reductase (Sigma, St. Louis, MO) in the reaction buffer (0.3 mmol/l insulin, 200 μmol/l NADPH, 1 mmol/l EDTA, and 20 mmol/l HEPES pH 7.6) at 37°C for 20 min. The reaction was terminated by adding stop mix (6 mol/l guanidine HCl and 1 mmol/l DTNB in 0.2M Tris-HCl, pH 8.0), and the absorption at 412 nm was measured. Relative Trx activities were quantified after normalization with total protein and expressed as the percentage of the nontreatment control subjects.

Animal study. Four-week-old apolipoprotein-E knockout (ApoE−/−) male mice (The Jackson Laboratory, Bar Harbor, ME) were fed a high-fat diet (Research Diets, New Brunswick, NJ) for 4 weeks and then subcutaneously injected with AICAR (0.5 mg/g body weight per day) or an equivalent volume of normal saline for 2 days. Mice were killed 24 h later. The aortas were irrigated with PBS, collected, and preserved at −80°C until used; alternatively, the aortas were fixed in 4% paraformaldehyde for the immunochemistry assay or optimal cutting temperature compound for ROS detection. All experiments were approved by the Animal Care Research at Baylor College of Medicine.

Statistical analysis. All quantitative variables are presented as the means ± SE from three separate experiments. We compared the differences of three or more groups with one-way ANOVA. Two-tailed $P < 0.05$ was considered statistically significant.

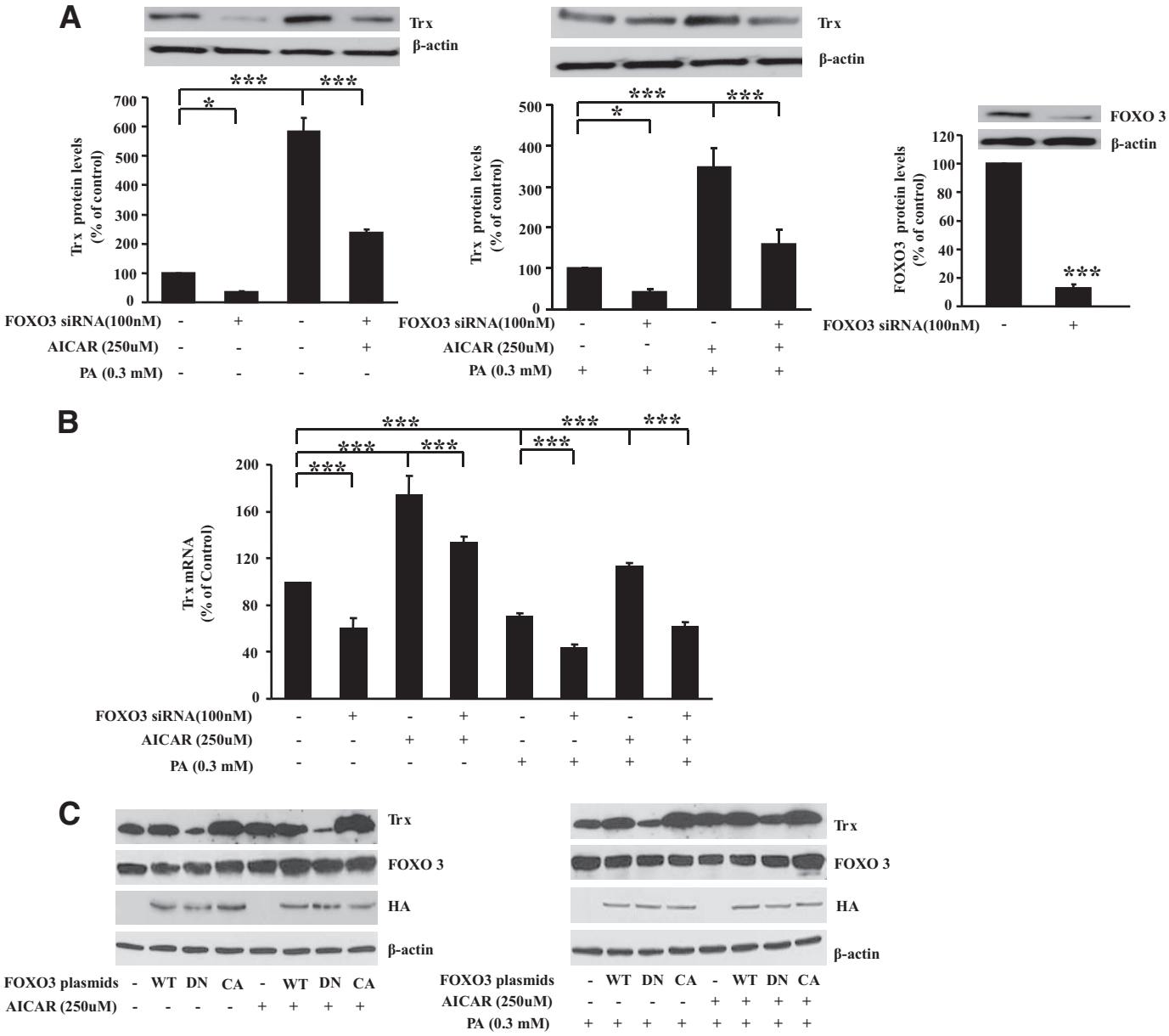

FIG. 5. FOXO3 mediated the AMPK-induced upregulation of Trx. *A*: Involvement of FOXO3 in basal and AICAR-regulated Trx protein expression. HAECs were transfected with FOXO3 siRNA and then treated with AICAR in the absence or the presence of palmitic acid (PA) for 24 h. The effectiveness of FOXO3 knockdown was examined by anti-FOXO3 antibody. Trx protein was measured by Western blot. Representative data and quantitative analysis from three independent experiments are shown. *$P < 0.05$, ***$P < 0.001$. FOXO3 siRNA decreased basal Trx protein levels and reversed the AICAR-mediated induction of Trx protein. *B*: Involvement of FOXO3 in basal and AICAR-regulated Trx mRNA expression. HAECs were transfected with FOXO3 siRNA and then treated with AICAR in the absence or the presence of palmitic acid for 24 h. Trx mRNA was examined by RT-PCR. Data represent the means ± SE ($N = 3$). ***$P < 0.001$. FOXO3 siRNA decreased basal Trx mRNA levels and reversed the AICAR-mediated induction of Trx mRNA. *C*: Overexpression of FOXO3 increased Trx protein levels. HSMCs were transfected with wild-type (HA-FOXO3a WT), constitutively active (HA-FOXO3a CA), or dominant-negative (HA-FOXO3a DN) FOXO3a. The transfection effectiveness was determined by anti-HA antibody. The expression of Trx, FOXO3, and β-actin was examined. Representative blots from three independent experiments are shown.

RESULTS

AMPK reduced ROS levels induced by palmitic acid in endothelial cells. We first tested whether activation of the AMPK pathway could reduce FFA-induced ROS production. HAECs were incubated with increasing amounts of AICAR in the presence or absence of palmitic acid; ROS levels were detected in the treated cells. As shown in Fig. 1*A*, AICAR treatment alone had minimal effects on basal ROS levels. Palmitic acid significantly increased intracellular ROS levels, an observation consistent with previous reports (23). The palmitic acid–induced increase in intracellular ROS levels was reduced by AICAR in a dose-dependent manner with up to a 60% reduction at the highest dose (500 μmol/l). This result indicates that activation of AMPK can reduce intracellular ROS levels. Additionally, suppression of AMPK by specific siRNAs not only increased basal ROS levels, but also augmented the palmitic acid–induced increase in ROS levels (Fig. 1*B*). Furthermore, the AICAR-induced reduction in ROS levels was abolished by AMPK siRNA. These data suggest that the AMPK pathway is capable of reducing intracellular ROS levels under basal conditions and when induced by palmitic acid.

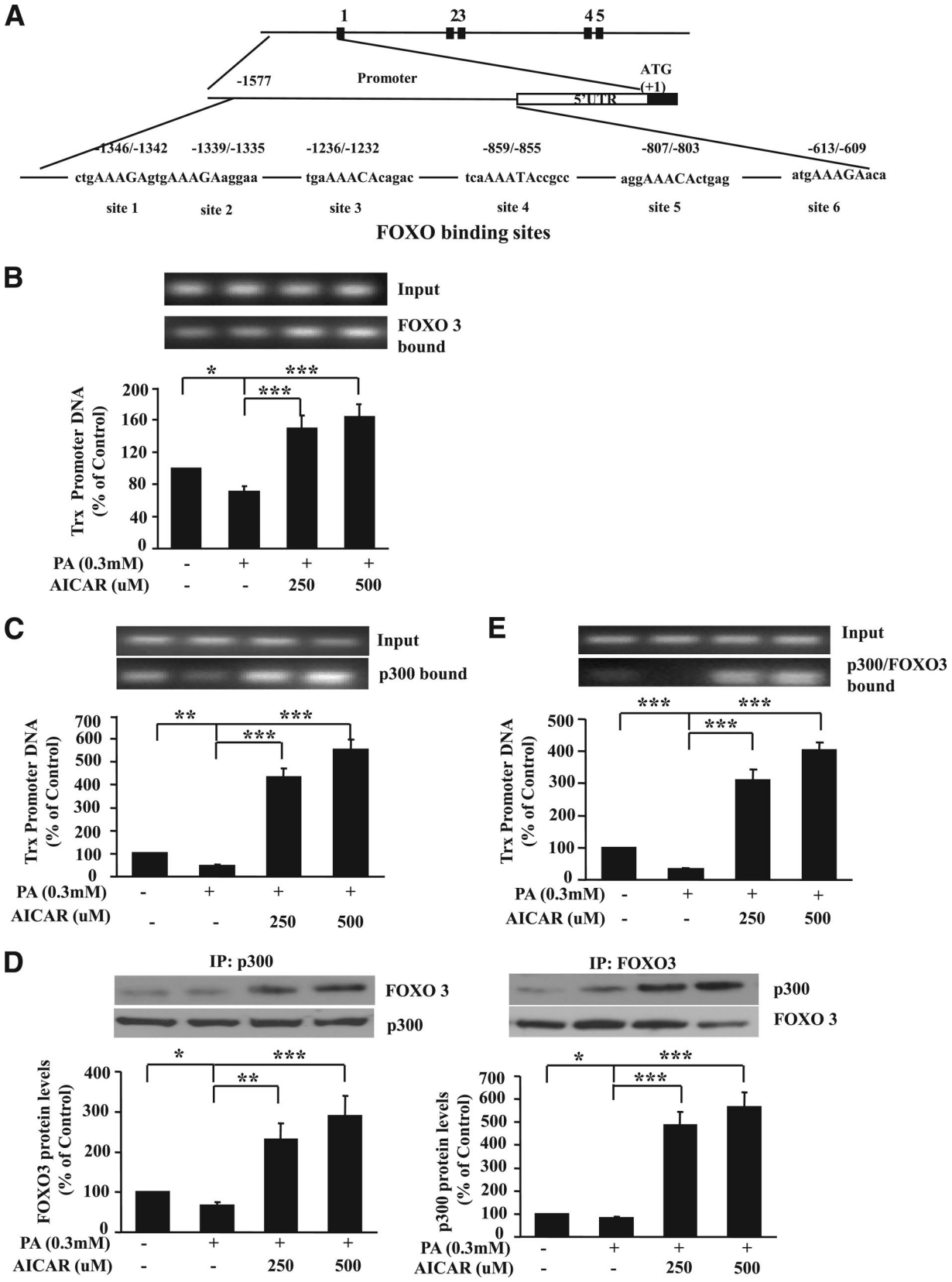

FIG. 6. AMPK promoted FOXO3 binding to the Trx promoter and formation of the FOXO3/p300 transcription complex in the *Trx* promoter. *A*: Depiction of FOXO binding sites in the *Trx* promoter. *B*: AICAR increased binding of FOXO3 to the *Trx* promoter. HAECs were treated with AICAR and palmitic acid (PA) for 24 h. FOXO3-DNA complexes were cross-linked by formaldehyde and immunoprecipitated with anti-FOXO3 antibody. Bound FOXO3 sites in the *Trx* promoter were detected by qPCR and normalized with input DNA. Relative DNA was compared and expressed as the percentage of the nontreatment control subjects. Representative blots and quantitative analysis from three independent experiments are shown. Data represent the means ± SE. *$P < 0.05$, ***$P < 0.001$ versus palmitic acid treatment. *C*: AICAR increased recruitment of p300 to the *Trx* promoter. HAECs were treated with AICAR and palmitic acid for 24 h. The protein-DNA complex was immunoprecipitated with an anti-p300 antibody. The FOXO binding site in the DNA-protein complex was amplified by PCR. Representative blots and qPCR analysis from

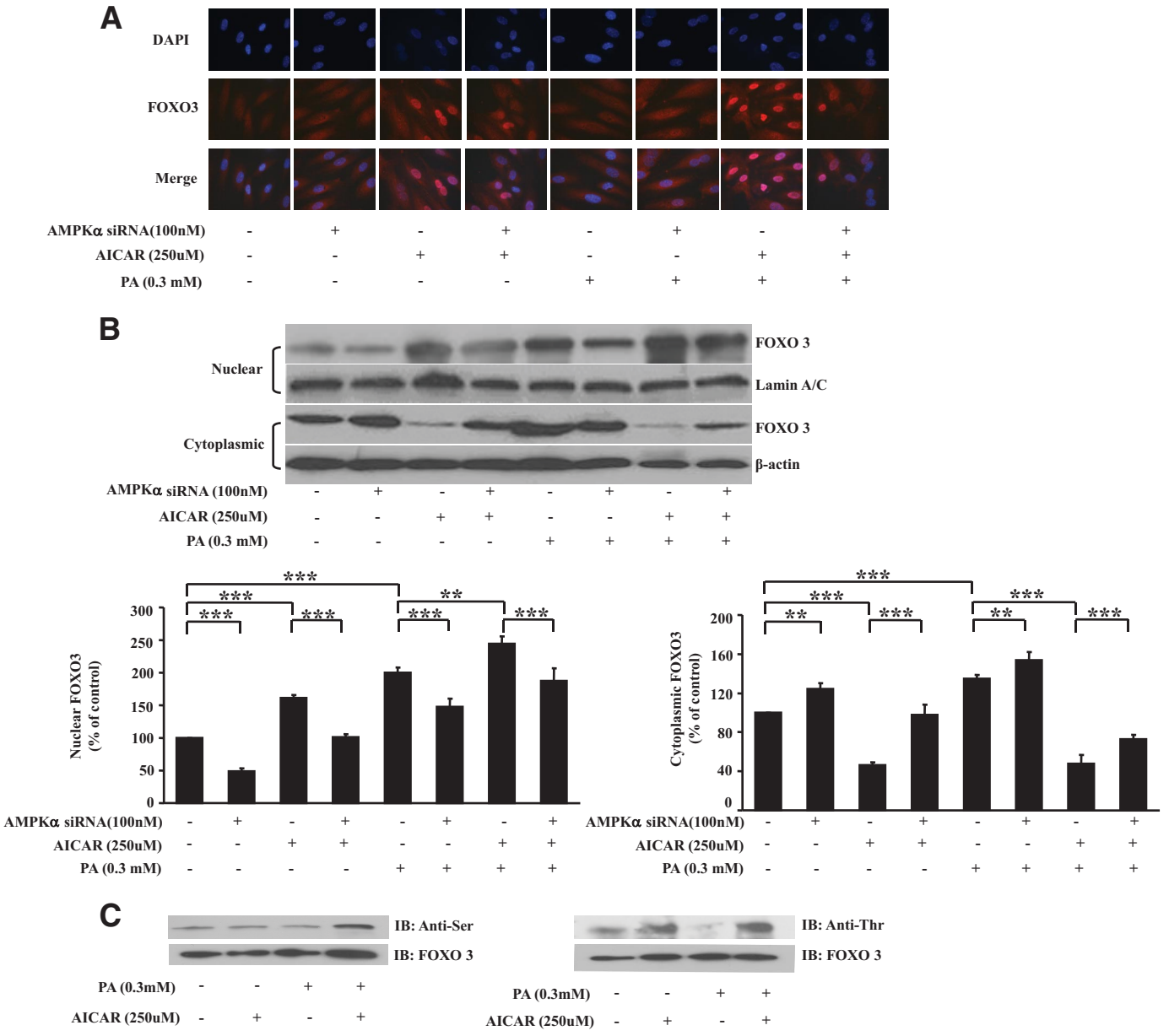

FIG. 7. AMPK promoted FOXO3 nuclear translocation. *A*: Effects of AMPK on FOXO3 cellular location. HAECs cultured on coverslips were transfected with AMPK siRNA and then treated with AICAR in the absence or presence of palmitic acid (PA) for 24 h. Treated cells were stained with an anti-FOXO3 antibody Texas Red (red) and DAPI (blue). Merged image shows colocalization. Representative images from three independent experiments are shown. AICAR increased FOXO3 nuclear translocation, which was prevented by AMPK siRNA. *B*: HAECs were transfected with AMPK siRNA and then treated with AICAR in the absence or presence of palmitic acid for 24 h. Nuclear and cytoplasmic proteins were extracted and the levels of FOXO3 were examined with an anti-FOXO3 antibody and normalized with β-actin or lamin A/C. Representative blots and quantitative analysis from three independent experiments are shown. Data represent the means ± SE ($N = 3$). $^{**}P < 0.01$, $^{***}P < 0.001$. *C*: AMPK directly phosphorylated FOXO3 in vitro. HAECs were treated with AICAR and palmitic acid for 24 h. AMPK was precipitated from the cell lysate using an anti-AMPK antibody and then incubated with recombinant FOXO3 in kinase assay buffer supplemented with ATP. Samples were separated on SDS-PAGE gel and transferred to PVDF membranes. Anti-serine (Anti-Ser) and anti-threonine (Anti-Thr) antibodies detected phosphorylation incorporated into the FOXO3. AICAR increased FOXO3 phosphorylation. Representative blots and quantitative analysis from three independent experiments are shown. (A high-quality digital representation of this figure is available in the online issue.)

AMPK increases the expression of the antioxidant Trx. We investigated whether the AMPK pathway could reduce ROS levels through Trx. First, we examined whether the AMPK pathway could regulate Trx expression. As shown in Fig. 2*A*, activation of the AMPK pathway by AICAR significantly upregulated expression of Trx in

three independent experiments are shown. Data represent the means ± SE ($N = 3$). $^{**}P < 0.01$, $^{***}P < 0.001$. *D*: AICAR increased FOXO3 and p300 association. The FOXO3 and p300 complex was coimmunoprecipitated with an anti-FOXO3 antibody, and p300 was detected by an anti-p300 antibody. Alternatively, the complex was immunoprecipitated with an anti-p300 antibody, and FOXO was detected by an anti-FOXO3 antibody. Representative blots and quantitative analysis from three independent experiments are shown. $^{*}P < 0.05$, $^{**}P < 0.01$, $^{***}P < 0.001$. *E*: AICAR increased binding of the FOXO3 and p300 complex in the *Trx* promoter. HAECs were treated with AICAR and palmitic acid for 24 h. The protein-DNA complex cross-linked by formaldehyde was first immunoprecipitated with an anti-FOXO3 antibody and then with an anti-p300 antibody. The FOXO site on the *Trx* promoter was detected by PCR. Representative blots and quantitative RT-PCR analysis from three independent experiments are shown. Data represent the means ± SE ($N = 3$). $^{***}P < 0.001$.

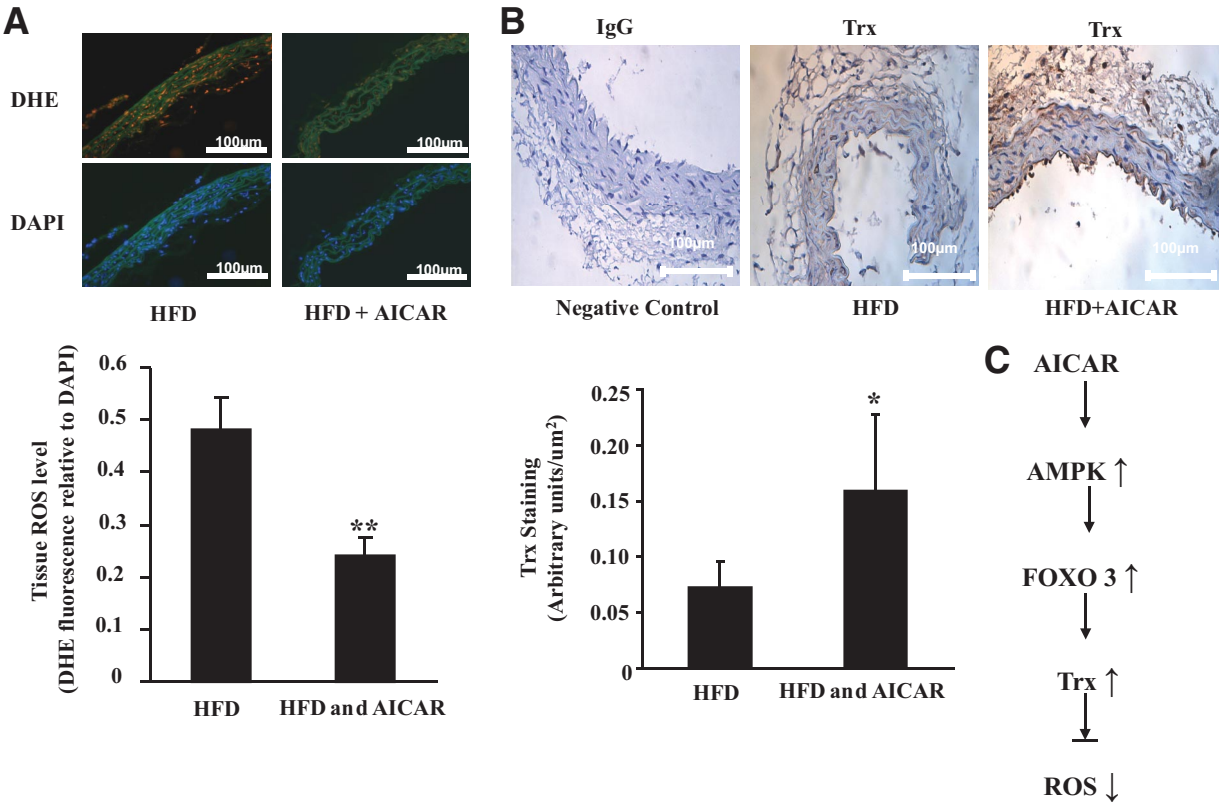

FIG. 8. AICAR increased Trx expression and decreased ROS levels in ApoE−/− mice fed a high-fat diet. ApoE−/− mice were fed a high-fat diet for 4 weeks and then injected with either 0.9% saline or AICAR (0.5 mg/g body weight per day) for 2 days. *A*: Superoxide O_2^- in the aortas was detected with DHE staining (red), and nuclei were conterstained with DAPI (blue). The relative ROS levels were estimated from the ratio of ethidium/DAPI fluorescence. The mean fluorescent intensity randomly selected from three fields per vessel was calculated. Results are means ± SE (n = 5). **P < 0.01 versus no AICAR control. *B*: Trx protein was detected with immunohistochemical staining. The signal density was normalized with vascular area and expressed as arbitrary units per micrometers squared. The mean fluorescent intensity randomly selected from three fields per vessel was calculated. Representative staining and quantitative analysis from each group are shown (n = 5). Results are means ± SE (n = 5). *P < 0.05 versus no AICAR control. *C*: Schematic diagram of the possible mechanism for the AMPK-mediated reduction in ROS levels. Activation of the AMPK pathway triggers phosphorylation and nuclear translocation of the transcription factor FOXO3, which can bind to the *Trx* promoter and promote Trx transcription. Increased Trx expression leads to a reduction in ROS levels. (A high-quality digital representation of this figure is available in the online issue.)

the absence and presence of palmitic acid. Although palmitic acid itself transiently increased Trx expression (data not shown), prolonged palmitic acid exposure decreased Trx expression. Importantly, knockdown of AMPKα by its specific siRNA inhibited both basal and AICAR-induced Trx expression (Fig. 2*B*), implicating that the AMPK pathway is involved in upregulating Trx. Consistent with this expression pattern, AICAR significantly increased total cellular Trx activity in the absence and presence of palmitic acid (Fig. 2*C*). Taken together, these data suggest that activation of AMPK increases Trx expression.

Trx silencing prevents the AICAR-induced reduction in ROS levels. We determined whether Trx is involved in the AMPK-induced reduction in ROS levels. Trx expression was silenced by Trx siRNA, and the effect of AMPK on ROS levels in Trx knockdown cells was examined. As shown in Fig. 3, Trx siRNA not only increased basal ROS levels, but also amplified the palmitic acid–induced increase in ROS levels. Furthermore, Trx siRNA prevented the AICAR-induced reduction in ROS levels. These data suggest that Trx is capable of reducing intracellular ROS levels and is involved in the APMK-mediated reduction in ROS levels.

AMPK regulates Trx expression at the mRNA level. To further explore the mechanisms of AMPK-induced upregulation of Trx expression, we examined whether AICAR could affect Trx transcription. Using qRT-PCR, we found that AICAR significantly increased Trx mRNA in a dose-dependent manner (Fig. 4*A*). Knockdown of AMPKα by its specific siRNA reduced basal Trx expression (Fig. 4*B*). Moreover, AICAR-induced Trx mRNA was reduced in the presence of AMPK siRNA. These results indicate that AMPK increases Trx expression at the mRNA level.

FOXO3 is required for the AMPK-induced upregulation of Trx. We investigated the mechanisms responsible for the AMPK-mediated upregulation of Trx. The 5′ flanking region of the human *Trx* gene contains consensus-binding sites for many transcription factors. We identified FOXO3 as one of these transcriptional factors that may mediate AMPK-induced Trx transcription. Silencing FOXO3 with siRNA significantly prevented the AICAR-induced expression of Trx at both the protein (Fig. 5*A*) and mRNA level (Fig. 5*B*), indicating that FOXO3a is involved in the AMPK-induced upregulation of Trx. Furthermore, overexpression of constitutively active FOXO3a (FOXO3a CA) significantly increased Trx expression in the absence or presence of AICAR, but domain-negative FOXO3a (FOXO3a DN) dramatically decreased Trx expression (Fig. 5*C*), further suggesting that FOXO3a is capable of upregulating Trx expression. Together, these data support the critical role of FOXO3 in the AMPK-induced upregulation of Trx.

FOXO3 binds directly to the *Trx* promoter, recruits p300, and forms a transcription activator complex on the *Trx* promoter. To examine whether FOXO3 directly induces Trx transcription, we examined whether FOXO3 binds to the *Trx* promoter in vivo. FOXO binds to the consensus site 5′-(C/G)(A/T)AAA(C/T)A-3′ (24). The promoter region in the *Trx* gene contains six putative FOXO binding sites (tgAAAGAgtga at −1346/−1342, tgAAAGAagga at −1339/−1335, gaAAACAcaga at −1236/−1232, caAAATAccgc at −859/−855, ggAAACActga at −807/−803, and tgAAAGAacag at −613/−609) (Fig. 6*A*). Results of the ChIP assay performed with a FOXO3 antibody showed that FOXO3 strongly bound to site 6 (Fig. 6*B*). Importantly, the binding of FOXO3 to the *Trx* promoter was significantly increased by AICAR treatment (Fig. 6*B*, $P < 0.001$), further suggesting that FOXO3 may mediate AMPK-induced Trx transcription.

We examined how the transcription factor FOXO3 binds to the *Trx* promoter and induces gene expression. One possible mechanism is chromatin remodeling in which transcription factors bind to a promoter and recruit histone acetylases (e.g., p300) that acetylate histones, unwind chromatin, and induce gene transcription. To test whether this mechanism applied to the FOXO3-mediated transcription activation of the *Trx* gene, we first examined whether p300 could bind to the *Trx* promoter. By using the ChIP assay, we found that AICAR treatment significantly increased p300 binding to the *Trx* promoter (Fig. 6*C*). We then examined whether FOXO3 was associated with p300 in vivo. By using a coimmunoprecipitation assay, we observed that FOXO3 was associated with p300 and that this association was increased by AICAR treatment (Fig. 6*D*), indicating that p300 recruitment to the *Trx* promoter may be mediated at least in part by FOXO3. Furthermore, the double-ChIP assay (Fig. 6*E*) showed that FOXO and p300 were in the same transcription complex in the *Trx* promoter, and this association was increased by AICAR treatment. Together, these results suggest that activated FOXO3 may recruit p300 and form a transcription activation complex in the *Trx* promoter, a process that can be promoted by the AMPK pathway.

AMPK increases FOXO3 nuclear translocation. We investigated the potential mechanisms by which AMPK regulates FOXO3. The immunostaining assay (Fig. 7*A*) and Western blot (Fig. 7*B*) showed that AICAR significantly increased the translocation of FOXO3 from the cytoplasm to the nucleus, which was prevented by AMPKα siRNA. We also examined whether AMPK could directly phosphorylate FOXO3. The in vitro kinase assay, with purified AMPK as the kinase and recombinant FOXO3 as the substrate, showed that AMPK directly phosphorylated FOXO3 at serine and threonine sites and that AICAR increased threonine phosphorylation of FOXO3 (Fig. 7*C*). These results indicate that FOXO3 may be phosphorylated by AMPK and subsequently translocate into the nucleus where it binds the *Trx* promoter and increases *Trx* transcription.

AICAR increases Trx expression and decreases ROS levels in vivo. Finally, we examined whether AMPK activation could affect the expression of Trx and, thus, reduce ROS levels in vivo. We used ApoE−/− mice fed a high-fat diet, a model that can produce metabolic disturbances, ROS overproduction, and vascular changes similar to those seen in metabolic syndrome. These mice were injected with either saline or AICAR (0.5 mg/g body weight per day) for 2 days; ROS levels and Trx expression in the aorta were compared. As shown in Fig. 8, the AICAR injection decreased ROS levels (Fig. 8*A*) and increased expression of Trx in the aortic wall (Fig. 8*B*), suggesting that activation of the AMPK pathway may enhance Trx expression and subsequently reduce ROS levels in the vascular wall.

DISCUSSION

In the present study, we showed that activation of AMPK reduces ROS levels by inducing expression of the antioxidant Trx. The transcriptional factor FOXO3 mediated the induction of transcription. AMPK activates FOXO3 by promoting its nuclear translocation, *Trx* promoter binding, and subsequently transcription complex formation. Based on these findings, we propose a pathway of the AMPK-mediated reduction of intracellular ROS (Fig. 8*C*).

Fatty acids are fuels that are used to efficiently generate ATP primarily through β-oxidation. However, when fatty acids are present in excessive amounts, along with increased oxidation and energy generation, they produce increased ROS, which contribute significantly to the pathogenesis of microvascular and macrovascular complications in diabetes (25,26). Strategies to decrease intracellular ROS levels and oxidative damage may have therapeutic potential in treating diabetes and its complications.

Our finding that activation of the AMPK pathway reduced intracellular ROS levels is consistent with previous reports (7–10). The AMPK pathway acts as a fuel gauge by switching on catabolic pathways for ATP generation when energy is depleted, a process coupled to the increase in ROS production. It has been shown that ROS can activate the AMPK pathway (5–7). The ability of AMPK to reduce ROS levels counterbalances the overproduction of ROS during fatty acid consumption. Reducing fatty acid–induced increases in ROS levels in endothelial cells may be an important mechanism in AMPK-mediated cardiovascular protection. Additionally, AMPK regulates endothelial function (2), angiogenesis (27), and the cell cycle (28). Moreover, AMPK also inhibits vascular inflammation (3), prevents endothelial injury induced by hyperglycemia and FFAs (4), and reduces myocardial infarction (29). Thus, upregulating this pathway may provide therapeutic benefits by not only reducing lipid storage and insulin resistance, but also preventing cardiovascular complications in metabolic syndrome.

We studied the mechanisms involved in the AMPK-mediated reduction in ROS. Decreasing intravascular ROS levels can be achieved by preventing the generation of or removing excess reactive species. Previous studies suggest that activation of the AMPK pathway normalizes hyperglycemia-induced ROS production by inducing manganese superoxide dismutase (8,30). We have shown for the first time that the AMPK pathway can decrease fatty acid–induced increases in intracellular ROS levels by upregulating Trx, a novel additional mechanism that explains AMPK's effects on reducing intracellular ROS. Trx is ubiquitously expressed in endothelial cells and protects the cells from ROS-induced cytotoxicity (15). Trx can also bind and inhibit apoptosis signal-regulating kinase 1 (31), an upstream kinase in the cellular stress–sensitive pathways (i.e., JNK and p38 pathways). Thus, upregulation of the Trx system by the AMPK pathway may be an important protective mechanism against excessive oxidative stress and the activation of stress-signaling pathways in the body.

Regarding how the AMPK pathway induces Trx expression, our study suggests that FOXO3 may be a target transcription factor that mediates AMPK's effects on Trx expression and ROS reduction. FOXO transcription factors are important regulators of metabolism, cell-cycle progression, apoptosis, and oxidative stress resistance. Recent findings suggest that ROS can activate FOXO (33–37). Although FOXOs mediate ROS-induced apoptosis (37,38) under lethal conditions, they can increase cell survival in response to physiologic oxidative stress (32,39–42), a function that is required for long-term regenerative potential and cell longevity (41,43).

The mechanisms whereby FOXO3 reduces ROS levels are not well defined. It has been shown that FOXO3 may be involved in the induction of catalase (44). Our study shows that FOXO3 reduces intracellular ROS levels by directly inducing the antioxidant Trx. When activated by AMPK, FOXO3 directly binds to the *Trx* promoter and forms a transcriptional complex on the *Trx* promoter, which may lead to activation of Trx transcription. However, further site-directed mutagenesis studies are needed to determine whether FOXO3 indeed targets site 6 and induces the transcriptional complex formation in the *Trx* promoter and whether this site is important for FOXO3-mediated *Trx* promoter transactivation. Together, these findings indicate the importance of FOXO3 in reducing ROS levels and protecting cells.

Increasing evidence suggests that AMPK can directly phosphorylate FOXO3, which mediates AMPKs ability to reduce cell stress and increase cell survival (45,46). Greer and colleagues have recently shown that AMPK directly phosphorylates at least six residues in the C-terminal domain of FOXO3, which activates the FOXO3 transcription factor (45). Our results support their findings. We showed that activation of AMPK by AICAR induced the nuclear translocation of FOXO3 and the binding of FOXO3 to the *Trx* promoter. Further studies will be necessary to define the detailed mechanisms of FOXO3 regulation by the AMPK pathway in response to metabolic stress.

In summary, using both in vitro and in vivo experiments we have shown that activation of the AMPK pathway significantly reduced palmitic acid–induced intracellular ROS levels by increasing the expression of the antioxidant Trx. The transcriptional factor FOXO3 mediated AMPK's effect on Trx expression. AMPK upregulated Trx transcription by increasing the nuclear translocation of FOXO3 and by promoting its binding to the *Trx* promoter. The AMPK-FOXO pathway has protective effects against cellular superoxide levels induced by metabolic stress and could be a therapeutic target when treating cardiovascular diseases in metabolic syndrome.

ACKNOWLEDGMENTS

This study was supported by American Heart Association Grants AHA-TX 0565134Y (to Y.H.S.) and AHA-0730190N (to Y.H.S.), National Institutes of Health Grant R01-HL071608 (to X.L.W.), and Natural Science Foundation of China Grants 2006CB503803 and 2006AA02A406 (to Y.Z.).

No potential conflicts of interest relevant to this article were reported.

Parts of this study were presented in abstract form at the 68th Scientific Sessions of the American Diabetes Association, San Francisco, California, 6–10 June 2008.

We acknowledge Hilary D. Marks, PhD, of the Texas Heart Institute at St. Luke's Episcopal Hospital, for her editorial assistance.

REFERENCES

1. Madamanchi NR, Runge MS. Mitochondrial dysfunction in atherosclerosis. Circ Res 2007;100:460–473
2. Zou MH, Hou XY, Shi CM, Nagata D, Walsh K, Cohen RA. Modulation by peroxynitrite of Akt- and AMP-activated kinase-dependent Ser1179 phosphorylation of endothelial nitric oxide synthase. J Biol Chem 2002;277:32552–32557
3. Gaskin FS, Kamada K, Yusof M, Korthuis RJ. 5′-AMP-activated protein kinase activation prevents postischemic leukocyte-endothelial cell adhesive interactions. Am J Physiol Heart Circ Physiol 2007;292:H326–H332
4. Ido Y, Carling D, Ruderman N. Hyperglycemia-induced apoptosis in human umbilical vein endothelial cells: inhibition by the AMP-activated protein kinase activation. Diabetes 2002;51:159–167
5. An Z, Wang H, Song P, Zhang M, Geng X, Zou MH. Nicotine-induced activation of AMP-activated protein kinase inhibits fatty acid synthase in 3T3L1 adipocytes: a role for oxidant stress. J Biol Chem 2007;282:26793–26801
6. Blattler SM, Rencurel F, Kaufmann MR, Meyer UA. In the regulation of cytochrome P450 genes, phenobarbital targets LKB1 for necessary activation of AMP-activated protein kinase. Proc Natl Acad Sci U S A 2007;104:1045–1050
7. Zhang M, Dong Y, Xu J, Xie Z, Wu Y, Song P, Guzman M, Wu J, Zou MH. Thromboxane receptor activates the AMP-activated protein kinase in vascular smooth muscle cells via hydrogen peroxide. Circ Res 2008;102:328–337
8. Kukidome D, Nishikawa T, Sonoda K, Imoto K, Fujisawa K, Yano M, Motoshima H, Taguchi T, Matsumura T, Araki E. Activation of AMP-activated protein kinase reduces hyperglycemia-induced mitochondrial reactive oxygen species production and promotes mitochondrial biogenesis in human umbilical vein endothelial cells. Diabetes 2006;55:120–127
9. Ouedraogo R, Wu X, Xu SQ, Fuchsel L, Motoshima H, Mahadev K, Hough K, Scalia R, Goldstein BJ. Adiponectin suppression of high-glucose-induced reactive oxygen species in vascular endothelial cells: evidence for involvement of a cAMP signaling pathway. Diabetes 2006;55:1840–1846
10. Ceolotto G, Gallo A, Papparella I, Franco L, Murphy E, Iori E, Pagnin E, Fadini GP, Albiero M, Semplicini A, Avogaro A. Rosiglitazone reduces glucose-induced oxidative stress mediated by NAD(P)H oxidase via AMPK-dependent mechanism. Arterioscler Thromb Vasc Biol 2007;27:2627–2633
11. Yamawaki H, Haendeler J, Berk BC. Thioredoxin: a key regulator of cardiovascular homeostasis. Circ Res 2003;93:1029–1033
12. Berndt C, Lillig CH, Holmgren A. Thiol-based mechanisms of the thioredoxin and glutaredoxin systems: implications for diseases in the cardiovascular system. Am J Physiol Heart Circ Physiol 2007;292:H1227–H1236
13. Okuda M, Inoue N, Azumi H, Seno T, Sumi Y, Hirata K, Kawashima S, Hayashi Y, Itoh H, Yodoi J, Yokoyama M. Expression of glutaredoxin in human coronary arteries: its potential role in antioxidant protection against atherosclerosis. Arterioscler Thromb Vasc Biol 2001;21:1483–1487
14. Zhang H, Luo Y, Zhang W, He Y, Dai S, Zhang R, Huang Y, Bernatchez P, Giordano FJ, Shadel G, Sessa WC, Min W. Endothelial-specific expression of mitochondrial thioredoxin improves endothelial cell function and reduces atherosclerotic lesions. Am J Pathol 2007;170:1108–1120
15. Shioji K, Kishimoto C, Nakamura H, Masutani H, Yuan Z, Oka S, Yodoi J. Overexpression of thioredoxin-1 in transgenic mice attenuates adriamycin-induced cardiotoxicity. Circulation 2002;106:1403–1409
16. Yamamoto M, Yang G, Hong C, Liu J, Holle E, Yu X, Wagner T, Vatner SF, Sadoshima J. Inhibition of endogenous thioredoxin in the heart increases oxidative stress and cardiac hypertrophy. J Clin Invest 2003;112:1395–1406
17. Turoczi T, Chang VW, Engelman RM, Maulik N, Ho YS, Das DK. Thioredoxin redox signaling in the ischemic heart: an insight with transgenic mice overexpressing Trx1. J Mol Cell Cardiol 2003;35:695–704
18. Tao L, Gao E, Bryan NS, Qu Y, Liu HR, Hu A, Christopher TA, Lopez BL, Yodoi J, Koch WJ, Feelisch M, Ma XL. Cardioprotective effects of thioredoxin in myocardial ischemia and reperfusion: role of S-nitrosation [corrected]. Proc Natl Acad Sci U S A 2004;101:11471–11476
19. Wang XL, Zhang L, Youker K, Zhang MX, Wang J, LeMaire SA, Coselli JS, Shen YH. Free fatty acids inhibit insulin signaling-stimulated endothelial nitric oxide synthase activation through upregulating PTEN or inhibiting Akt kinase. Diabetes 2006;55:2301–2310
20. Shen YH, Zhang L, Gan Y, Wang X, Wang J, Lemaire SA, Coselli JS, Wang XL. Up-regulation of PTEN (phosphatase and tensin homolog deleted on chromosome ten) mediates p38 MAPK stress signal-induced inhibition of insulin signaling: a cross-talk between stress signaling and insulin signaling

in resistin-treated human endothelial cells. J Biol Chem 2006;281:7727–7736
21. Shen YH, Godlewski J, Zhu J, Sathyanarayana P, Leaner V, Birrer MJ, Rana A, Tzivion G. Cross-talk between JNK/SAPK and ERK/MAPK pathways: sustained activation of JNK blocks ERK activation by mitogenic factors. J Biol Chem 2003;278:26715–26721
22. Schulze PC, Yoshioka J, Takahashi T, He Z, King GL, Lee RT. Hyperglycemia promotes oxidative stress through inhibition of thioredoxin function by thioredoxin-interacting protein. J Biol Chem 2004;279:30369–30374
23. Koshkin V, Wang X, Scherer PE, Chan CB, Wheeler MB. Mitochondrial functional state in clonal pancreatic β-cells exposed to free fatty acids. J Biol Chem 2003;278:19709–19715
24. Tsai KL, Sun YJ, Huang CY, Yang JY, Hung MC, Hsiao CD. Crystal structure of the human FOXO3a-DBD/DNA complex suggests the effects of post-translational modification. Nucleic Acid Res 2007;35:6984–6994
25. Tripathy D, Mohanty P, Dhindsa S, Syed T, Ghanim H, Aljada A, Dandona P. Elevation of free fatty acids induces inflammation and impairs vascular reactivity in healthy subjects. Diabetes 2003;52:2882–2887
26. Wyne KL. Free fatty acids and type 2 diabetes mellitus. Am J Med 2003;115(Suppl. 8A):29S–36S
27. Nagata D, Mogi M, Walsh K. AMP-activated protein kinase (AMPK) signaling in endothelial cells is essential for angiogenesis in response to hypoxic stress. J Biol Chem 2003;278:31000–31006
28. Guo D, Chien S, Shyy JY. Regulation of endothelial cell cycle by laminar versus oscillatory flow: distinct modes of interactions of AMP-activated protein kinase and Akt pathways. Circ Res 2007;100:564–571
29. Depre C, Wang L, Sui X, Qiu H, Hong C, Hedhli N, Ginion A, Shah A, Pelat M, Bertrand L, Wagner T, Gaussin V, Vatner SF. H11 kinase prevents myocardial infarction by preemptive preconditioning of the heart. Circ Res 2006;98:280–288
30. Civitarese AE, Ukropcova B, Carling S, Hulver M, DeFronzo RA, Mandarino L, Ravussin E, Smith SR. Role of adiponectin in human skeletal muscle bioenergetics. Cell Metab 2006;4:75–87
31. Saitoh M, Nishitoh H, Fujii M, Takeda K, Tobiume K, Sawada Y, Kawabata M, Miyazono K, Ichijo H. Mammalian thioredoxin is a direct inhibitor of apoptosis signal-regulating kinase (ASK) 1. Embo J 1998;17:2596–2606
32. Kops GJ, Dansen TB, Polderman PE, Saarloos I, Wirtz KW, Coffer PJ, Huang TT, Bos JL, Medema RH, Burgering BM. Forkhead transcription factor FOXO3a protects quiescent cells from oxidative stress. Nature 2002;419:316–321
33. Brunet A, Sweeney LB, Sturgill JF, Chua KF, Greer PL, Lin Y, Tran H, Ross SE, Mostoslavsky R, Cohen HY, Hu LS, Cheng HL, Jedrychowski MP, Gygi SP, Sinclair DA, Alt FW, Greenberg ME. Stress-dependent regulation of FOXO transcription factors by the SIRT1 deacetylase. Science 2004;303:2011–2015
34. van der Horst A, de Vries-Smits AM, Brenkman AB, van Triest MH, van den Broek N, Colland F, Maurice MM, Burgering BM. FOXO4 transcriptional activity is regulated by monoubiquitination and USP7/HAUSP. Nat Cell Biol 2006;8:1064–1073
35. Almeida M, Han L, Martin-Millan M, O'Brien CA, Manolagas SC. Oxidative stress antagonizes Wnt signaling in osteoblast precursors by diverting β-catenin from T cell factor- to forkhead box O-mediated transcription. J Biol Chem 2007;282:27298–27305
36. Owusu-Ansah E, Yavari A, Mandal S, Banerjee U. Distinct mitochondrial retrograde signals control the G1-S cell cycle checkpoint. Nat Genet 2008;40:356–361
37. Nakamura T, Sakamoto K. Forkhead transcription factor FOXO subfamily is essential for reactive oxygen species-induced apoptosis. Mol Cell Endocrinol 2008;281:47–55
38. Lehtinen MK, Yuan Z, Boag PR, Yang Y, Villen J, Becker EB, DiBacco S, de la Iglesia N, Gygi S, Blackwell TK, Bonni A. A conserved MST-FOXO signaling pathway mediates oxidative-stress responses and extends life span. Cell 2006;125:987–1001
39. Tothova Z, Kollipara R, Huntly BJ, Lee BH, Castrillon DH, Cullen DE, McDowell EP, Lazo-Kallanian S, Williams IR, Sears C, Armstrong SA, Passegue E, DePinho RA, Gilliland DG. FoxOs are critical mediators of hematopoietic stem cell resistance to physiologic oxidative stress. Cell 2007;128:325–339
40. Marinkovic D, Zhang X, Yalcin S, Luciano JP, Brugnara C, Huber T, Ghaffari S. Foxo3 is required for the regulation of oxidative stress in erythropoiesis. J Clin Invest 2007;117:2133–2144
41. Hattangadi SM, Lodish HF. Regulation of erythrocyte lifespan: do reactive oxygen species set the clock? J Clin Invest 2007;117:2075–2077
42. Arden KC. FoxOs in tumor suppression and stem cell maintenance. Cell 2007;128:235–237
43. Zheng X, Yang Z, Yue Z, Alvarez JD, Sehgal A. FOXO and insulin signaling regulate sensitivity of the circadian clock to oxidative stress. Proc Natl Acad Sci U S A 2007;104:15899–15904
44. Alcendor RR, Gao S, Zhai P, Zablocki D, Holle E, Yu X, Tian B, Wagner T, Vatner SF, Sadoshima J. Sirt1 regulates aging and resistance to oxidative stress in the heart. Circ Res 2007;100:1512–1521
45. Greer EL, Oskoui PR, Banko MR, Maniar JM, Gygi MP, Gygi SP, Brunet A. The energy sensor AMP-activated protein kinase directly regulates the mammalian FOXO3 transcription factor. J Biol Chem 2007;282:30107–30119
46. Greer EL, Dowlatshahi D, Banko MR, Villen J, Hoang K, Blanchard D, Gygi SP, Brunet A. An AMPK-FOXO pathway mediates longevity induced by a novel method of dietary restriction in *C. elegans*. Curr Biol 2007;17:1646–1656